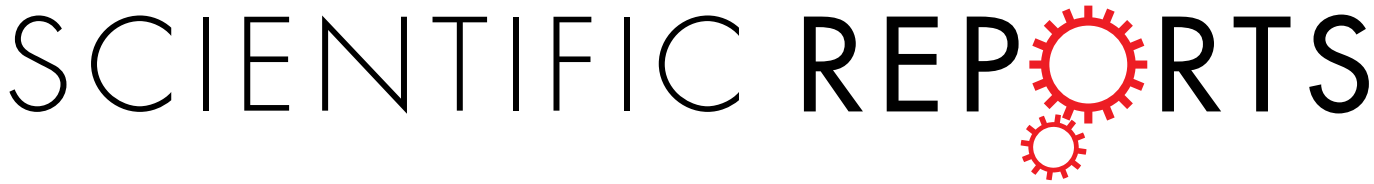

OPEN

High Elastic Moduli of a $54Al_2O_3$-$46Ta_2O_5$ Glass Fabricated via Containerless Processing

Received: 29 May 2015
Accepted: 09 September 2015
Published: 15 October 2015

Gustavo A. Rosales-Sosa[1], Atsunobu Masuno[1], Yuji Higo[2], Hiroyuki Inoue[1], Yutaka Yanaba[1], Teruyasu Mizoguchi[1], Takumi Umada[1], Kohei Okamura[1], Katsuyoshi Kato[1] & Yasuhiro Watanabe[1]

Glasses with high elastic moduli have been in demand for many years because the thickness of such glasses can be reduced while maintaining its strength. Moreover, thinner and lighter glasses are desired for the fabrication of windows in buildings and cars, cover glasses for smart-phones and substrates in Thin-Film Transistor (TFT) displays. In this work, we report a $54Al_2O_3$-$46Ta_2O_5$ glass fabricated by aerodynamic levitation which possesses one of the highest elastic moduli and hardness for oxide glasses also displaying excellent optical properties. The glass was colorless and transparent in the visible region, and its refractive index n_d was as high as 1.94. The measured Young's modulus and Vickers hardness were 158.3 GPa and 9.1 GPa, respectively, which are comparable to the previously reported highest values for oxide glasses. Analysis made using ^{27}Al Magic Angle Spinning Nuclear Magnetic Resonance (MAS NMR) spectroscopy revealed the presence of a significantly large fraction of high-coordinated Al in addition to four-coordinated Al in the glass. The high elastic modulus and hardness are attributed to both the large cationic field strength of Ta^{5+} ions and the large dissociation energies per unit volume of Al_2O_3 and Ta_2O_5.

Glasses with high elastic moduli and high hardness values have been in demand for many years because the thickness of sheet glass with these properties can be decreased while maintaining its strength. Thinner and lighter glasses are desired for windows in buildings and cars, substrates for TFT displays, and covers of smart-phones[1–3]. The elastic modulus and hardness of a glass can be estimated with relatively good accuracy using semi-empirical models based on ionic-pair potentials that consider the chemical composition, density, and selected physical property data[4–6]. Particularly, the Young's modulus E can be estimated using the Makishima and Mackenzie equation in which E is proportional to the atomic packing density and the sum of the partial dissociation energies of the components per unit volume[4,5]. The dissociation energies are in turn related to the bond strengths of the ionic pairs in the components. The Yamane and Mackenzie equation also indicates that the Vickers hardness (which is known to be directly related to the Young's Modulus) is proportional to the square root of the bulk modulus K, shear modulus G, and the bond strengths of the components[7]. Therefore, in order to achieve high elastic moduli and high hardness values, the use of components with large dissociation energies and a high atomic packing density are key factors.

Alumina (Al_2O_3) has one of the highest dissociation energies among the oxides ($G_{Al2O3} = 131\,kJ/cm^3$)[4]. Accordingly, high elastic modulus and high hardness glasses generally include large quantities of Al_2O_3, as is found in R_2O_3-Al_2O_3-SiO_2 glasses (R = rare earth ion, Y, or Sc)[8–11]. These glasses also have high atomic packing densities. However, because Al_2O_3 is considered an intermediate oxide according to Sun's glass formation criteria, the glass forming ability of a composition typically decreases as the quantity of Al_2O_3 increases[12]. In addition, compositions with a large amount of Al_2O_3 are often difficult to melt

[1]Institute of Industrial Science, The University of Tokyo, Tokyo, 153-8505, Japan. [2]Japan Synchrotron Radiation Research Institute, Hyogo, 679-5198, Japan. Correspondence and requests for materials should be addressed to A.M. (email: masuno@iis.u-tokyo.ac.jp)

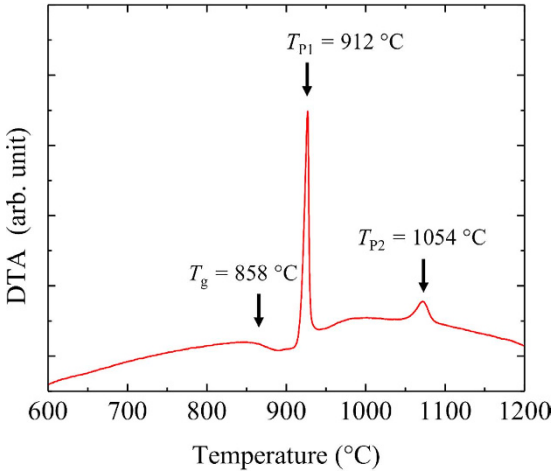

Figure 1. DTA curve for the $54Al_2O_3$-$46Ta_2O_5$ glass showing T_g, and the first (T_{P1}) and second crystallization peaks (T_{P2}).

due to their high melting temperatures. These issues have limited the fabrication of bulk glasses with high elastic moduli and high hardness values. Recent progress in containerless processing has, however, allowed the vitrification of low glass forming materials, including those without added network formers such as TiO_2-based, Nb_2O_5-based, WO_3-based, and Al_2O_3-based compositions, because heterogeneous nucleation from the melt can be avoided with this technique[13–18]. Thus, R_2O_3-Al_2O_3 glasses containing large quantities of Al_2O_3 have been prepared and found to exhibit superior mechanical properties as expected[19,20]. As a result, Al_2O_3-based glasses have attracted interest as high elastic moduli and high hardness materials. The properties of such glasses should be enhanced through the incorporation of additional components other than Al_2O_3 with high dissociation energies and high packing volumes. Herein, we describe the preparation of the new $54Al_2O_3$-$46Ta_2O_5$ glass, which exhibits high elastic moduli and hardness values, using containerless processing. The thermal, optical, and mechanical properties of the glass are also reported. In addition, an approach to the design of glasses with higher elastic moduli and higher hardness is proposed on the basis of the results of the local structure analysis around aluminum performed using ^{27}Al MAS NMR spectroscopy.

Results

Figure 1 shows the Differential Thermal Analysis (DTA) curve for the $54Al_2O_3$-$46Ta_2O_5$ glass. The glass transition temperature T_g is located at 858 °C, and the first T_{P1} and second T_{P2} crystallization peak are observed at 912 °C and 1054 °C, respectively. The difference between T_{P1} and T_g ($\Delta T = T_{P1} - T_g$) a measure of the thermal stability of the glass, is 54 °C, indicating the difficulty for vitrifying the glass using a conventional melting process. X-ray Diffraction (XRD) analysis confirmed that glass was totally amorphous and that the main phase of the crystallized sample after DTA was $AlTaO_4$. The density of the annealed glass was $\rho = 6.01\,g/cm^3$. The composition of the glass samples measured by x-ray fluorescence (XRF) showed that the changes with respect to the nominal composition were less than 1 mol%. The microstructure of the fabricated glasses investigated through high-angle annular dark field scanning transmission electron microscopy (HAADF-STEM) is shown in Fig. 2. Observation through the HAADF-STEM has the advantage of achieving chemical contrast at the nanometric scale because it is very sensitive to the atomic number[21]. From the figure it can be observed that the glass is homogeneous at different scales and no phase-separation is observed. The randomly distributed bright points at the highest magnification are associated with the Ta atoms which have a much larger atomic number compared with the Al atoms (dark regions).

Figure 3 shows the transmittance spectrum of the $54Al_2O_3$-$46Ta_2O_5$ glass in the ultraviolet-visible (UV/vis) region. The glass was transparent in the visible region and had a maximum apparent transmission of 81%. The maximum theoretical transmittance was also estimated to be 81% using the equation $R_{max} = 1-[2R'/(1+R')]$, where $R' = [(n_d-1)/(n_d+1)]^2$, and the experimental refractive index n_d value of the glass which was found to be 1.94. The estimated value was similar as that of the experimental result, indicating that the apparent transmittance value was to the result of losses only due to sample surface reflection, and no light scattering occurred in the glass[22]. As observed in the inset of Fig. 3, the glass is colorless and transparent, which confirms that the valence state for all of the Ta ions is five, and no Ta^{4+} ions are present[23]. The optical bandgap energy was estimated to be 4.3 eV using the UV absorption edge located at 288 nm.

The measured longitudinal velocity V_P and transversal velocity V_S of the $54Al_2O_3$-$46Ta_2O_5$ glass were 5.86 km/s and 3.20 km/s, respectively. From these values and the experimental density, it was found that the Young's modulus E was 158.3 GPa, the bulk modulus K was 124.1 GPa, the shear modulus G

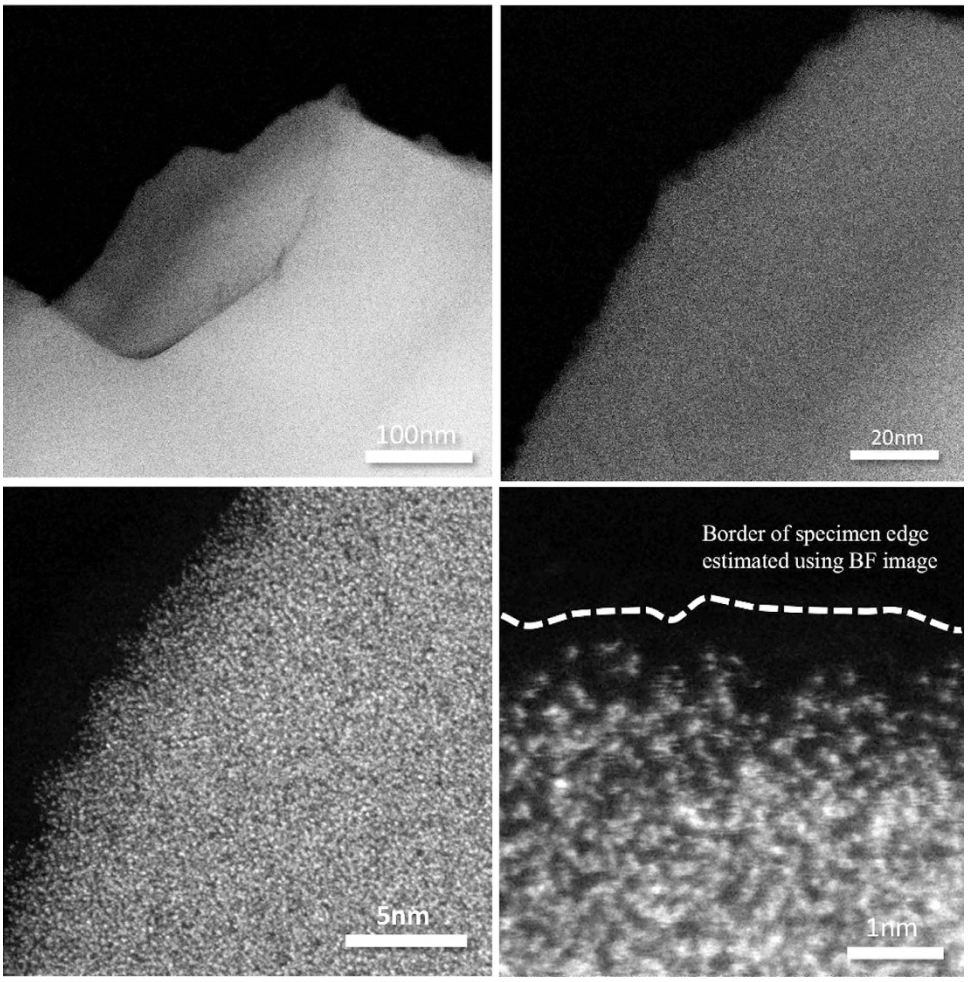

Figure 2. HAADF-STEM images at different magnifications for the $54Al_2O_3$-$46Ta_2O_5$ glasses.

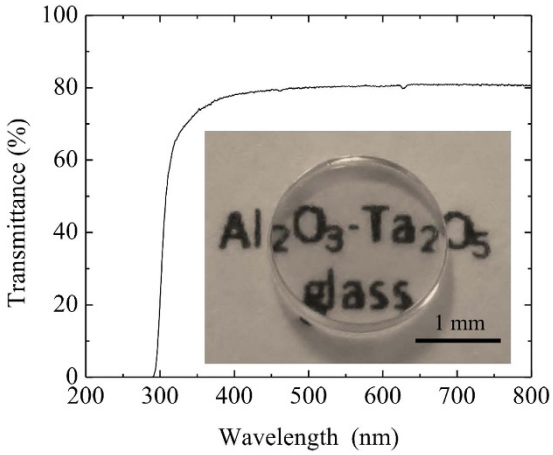

Figure 3. Transmittance spectrum of the $54Al_2O_3$-$46Ta_2O_5$ glass in the UV/vis region. The inset picture shows the glass sample used for the transmittance experiment.

was 61.5 GPa, and the Poisson's ratio v was 0.29. These values for the elastic moduli are considerably high and comparable to the maximum values in oxide glasses such as $40Y_2O_3$-$55Al_2O_3$-$5SiO_2$ and $28.5La_2O_3$-$71.5Al_2O_3$, whose Young's moduli were determined using Brillouin spectroscopy (169 GPa); however our measurement system showed that the Young's modulus of those glasses were 145.5 GPa and 123 GPa respectively[1,9,10]. The Vickers hardness of the $54Al_2O_3$-$46Ta_2O_5$ glass was 9.10 ± 0.05 GPa, which

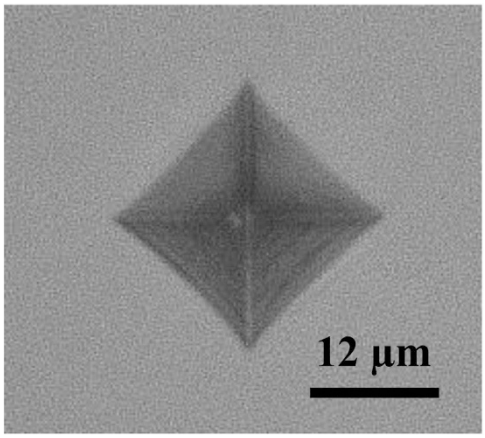

Figure 4. Vickers indentation imprint at 2.943 N for the $54Al_2O_3$-$46Ta_2O_5$ glass.

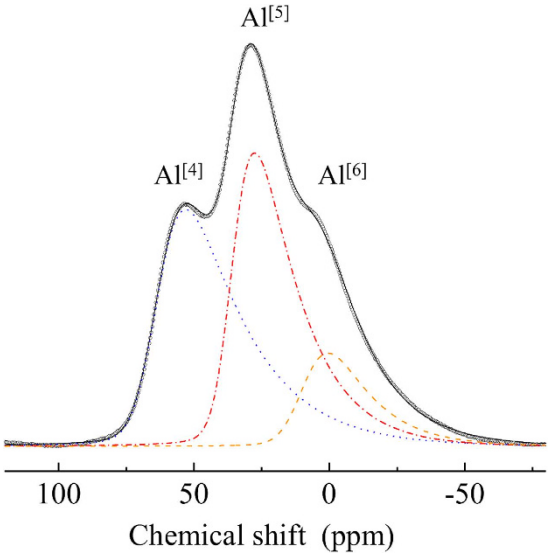

Figure 5. ^{27}Al MAS NMR spectrum of the $54Al_2O_3$-$46Ta_2O_5$ glass. The total fitting curve corresponds to the sum of three Czjzek fitting curves: blue dots ($Al^{[4]}$), red dashes and dots ($Al^{[5]}$), and orange dashes ($Al^{[6]}$).

is also comparable to the maximum values reported for the oxide glasses; $81.8Al_2O_3$-$18.2Y_2O_3$ (~9 GPa) and $29.3Al_2O_3$-$50.2SiO_2$-$20.5Sc_2O_3$ (9.4 GPa)[20,24]. Figure 4 shows indentation imprint for the $54Al_2O_3$-$46Ta_2O_5$ glass at a load of 2.942 N. Extensive lines due to shear deformation on each face of the imprints are observed. In addition, at the same load, some of the imprints exhibited radial crack behavior[25,26]. No cracks were observed in any indentation below 1 N. The indentation cracking resistance (*CR*) was estimated to be 2.50 ± 0.13 N, which is comparable to a commercial Vycor glass[27].

The ^{27}Al MAS NMR spectrum of the $54Al_2O_3$-$46Ta_2O_5$ glass is presented in Fig. 5. Although the spectrum is broad due to the amorphous nature of the glass, two distinctive peaks and a small shoulder were observed. These peaks and the shoulder were assigned to 4-coordinated Al ($Al^{[4]}$), 5-coordinated Al ($Al^{[5]}$), and 6-coordinated ($Al^{[6]}$), respectively[28–30]. The spectrum was decomposed into the three components using the "dmfit" program applying a simple Czjzek model[31,32]. The thin dotted lines in the spectrum correspond to each of the components. The fitting, values for δ_{iso} (isotropic chemical shift), dCSA (width of the Gaussian distribution of δ_{iso}), and νQ^* (quadrupolar product in kHz) were determined to be 64.8 ppm, 15 ppm, and 1134 kHz for $Al^{[4]}$; 36.7 ppm, 12 ppm, and 985 kHz for $Al^{[5]}$; and 10.3 ppm, 15 ppm, and 973 kHz for $Al^{[6]}$, respectively[33]. Based on the integration of the peak areas, the fractions of $Al^{[4]}$, $Al^{[5]}$, and $Al^{[6]}$ were estimated to be 44.1%, 41.9%, and 14.0%, respectively. The estimated average oxygen coordination number for Al was 4.7. The fractions of $Al^{[5]}$ and $Al^{[6]}$ were considerably larger than those observed in other aluminate glasses; Al typically forms AlO_4 tetrahedra in MO-Al_2O_3 (M = Ca, Sr and Ba) glasses[30]. While $Al^{[5]}$ and $Al^{[6]}$ have been observed in some Al_2O_3-containing glasses, such as R_2O_3-Al_2O_3 (R is a rare earth ion or Y), R_2O_3-Al_2O_3-SiO_2, and CaO-Al_2O_3-SiO_2, the fraction of $Al^{[5]}$

has generally ranged from 3 to 30%, and that of $Al^{[6]}$ from 1 to 2%[24,34,35]. The structure of the $54Al_2O_3$-$46Ta_2O_5$ glass may therefore be due to not only the presence of AlO_4 networks but also result in part from the high oxygen coordination of Al. The mechanism of glass formation with retention of large fractions of $Al^{[5]}$ and $Al^{[6]}$ is interesting and thus will be the subject of further investigations.

Discussion

These combined results indicate that the $54Al_2O_3$-$46Ta_2O_5$ glass have good mechanical properties, high transparency and a high refractive, with an unconventional amount of $Al^{[5]}$ and $Al^{[6]}$ species. In order to understand the origin of the good mechanical properties of the glass the results are analyzed within the context of the Makishima and Mackenzie model *e.g.* the atomic packing density and dissociation energy per unit volume of the glass components.

The atomic packing density C_g was calculated from the density using the formula $C_g = \rho(\Sigma x_i V_i)/M$, where M is the molecular weight of the glass and x_i is the molar fraction of the component i. The ionic volume V_i of an oxide is $N_A(4/3)(mr_A^3 + nr_O^3)$, where N_A is Avogadro's number, m and n are the number of atoms in the A_mO_n oxide, r_A is the ionic radius of the cation, and r_O is the ionic radius of oxygen. Shannon and Prewitt ionic radii were used[36]. The coordination numbers for Ta and O in the $54Al_2O_3$-$46Ta_2O_5$ glass were assumed to be 6 and 2, respectively, and the fractions of the coordination numbers for Al estimated from the results of the ^{27}Al MAS NMR were used. The atomic packing density C_g was found to be 0.586, which is significantly larger than those for conventional oxide glasses (i.e., for SiO_2 glass, C_g is 0.452). The small molar volume of Ta_2O_5 and the large fraction of highly coordinated Al are thought to contribute to the high packing density of the $54Al_2O_3$-$46Ta_2O_5$ glass. It has been suggested that the formation of highly coordinated Al in aluminate glasses is promoted by the large cationic field strength, as observed in R_2O_3-Al_2O_3-SiO_2 glasses[8–11]. Ta^{5+} also has large cationic field strength because of its small ionic radius and high valence state. Accordingly, Ta_2O_5 likely contributes to the high packing density of the $54Al_2O_3$-$46Ta_2O_5$ glass via the formation of a large number of highly coordinated Al atoms.

A high content of Ta_2O_5 is also characteristic of the $54Al_2O_3$-$46Ta_2O_5$ glass. The dissociation energy of Ta_2O_5 is substantially large (95.6 kJ/cm^3)[11]. The elastic moduli of the glass were estimated using the Makishima and Mackenzie equation given by $E = 2C_g(\Sigma x_i G_i)$. Here G_i is the dissociation energy of each component oxide. Values of 131 kJ/cm^3, 125 kJ/cm^3 and 119.2 kJ/cm^3 were used for G_{Al2O3} with Al in coordination of 4, 5, and 6 respectively[11,37,38]. The calculated Young's modulus E of the $54Al_2O_3$-$46Ta_2O_5$ glass was 131.9 GPa, which was approximately 17% less than the experimentally determined value, but still in relatively good agreement. A more accurate model may be necessary for estimation of the atomic packing density that includes the real contribution of the more highly coordinated cations. The energy contribution ratios of Al_2O_3 and Ta_2O_5 to the Young's modulus were also estimated using the Makishima and Mackenzie equation and found to be 62% and 38%, respectively. It should be noted that the contribution of Al_2O_2 is not that high, while that of Ta_2O_5 is considerably high, which is unlike most other binary aluminate glasses with high elastic moduli. For example, a $28.5La_2O_3$-$71.5Al_2O_3$ glass, which has one of the highest reported Young's modulus values among the oxide glasses, has the following contribution: 16.71% from La_2O_3 and 83.3% from Al_2O_3. It has been previously accepted that a large contribution by Al_2O_3 is necessary to achieve a high elastic modulus for binary aluminate glasses, such as $R_2O_3-Al_2O_3$. However, a simple estimation of the energy contribution of the components in $54Al_2O_3$-$46Ta_2O_5$ glass revealed that an appropriate component, like Ta_2O_5, can increase the elastic modulus even if the dissociation energy contribution of Al_2O_3 is small.

In summary, a glass with composition $54Al_2O_3$-$46Ta_2O_5$ was fabricated using an aerodynamic levitation technique. Its glass transition temperature T_g was 858 °C, and crystallization occurred at 54 °C above T_g, indicating a low glass forming ability. The glass is colorless and highly transparent in the visible region and has a refractive index n_d of 1.94. The Young's modulus E, bulk modulus K, shear modulus G, and Poisson's ratio ν of the $54Al_2O_3$-$46Ta_2O_5$ glass were determined via ultrasonic pulse-echo overlap analysis and were found to be 158.3 GPa, 124.1 GPa, 61.5 GPa, and 0.29, respectively, while the Vickers hardness of the glass was found to be 9.1 GPa. These elastic moduli and Vickers hardness values are quite high and comparable to the maximum values of conventional oxide glasses. In addition, an indentation cracking resistance of 2.5 N was estimated from the indentation experiments. Furthermore, ^{27}Al MAS NMR spectroscopic analysis revealed that the fractions of $Al^{[4]}$, $Al^{[5]}$, and $Al^{[6]}$ in the $54Al_2O_3$-$46Ta_2O_5$ glass were 44.1%, 41.9%, and 14.0%, respectively, and the average oxygen coordination number of the Al cations was 4.7. Notably, the fractions of $Al^{[5]}$ and $Al^{[6]}$ are considerably large compared to those observed in conventional oxide glasses, and may form because of the large cationic field strength of Ta^{5+}. These results indicated that Ta_2O_5 was a key contributor to the high elastic moduli and high hardness values of the glass because the addition of Ta_2O_5 increases the packing density via formation of Al atoms that are highly coordinated with oxygen and because the Ta_2O_5 itself has a large dissociation energy. Moreover, a simple estimation of the energy contributions of the components in the $54Al_2O_5$-$46Ta_2O_5$ glass using the Makishima and Mackenzie equation also suggested that the use of appropriate components can increase the elastic moduli even if the contribution of Al_2O_3 is small. These results provide insight into the design and fabrication of harder glasses based on both the local structure and the dissociation energies of the components.

Methods

Glass synthesis. Glasses were fabricated using an aerodynamic levitation furnace described elsewhere[23]. High-purity (99.99%) α-Al_2O_3 and Ta_2O_5 powders were mixed stoichiometrically with the chemical composition $54Al_2O_3$-$46Ta_2O_5$, pelletized using a hydrostatic press, and annealed at 1050 °C for 12 h in air. Pieces obtained from the crushed pellets were levitated in an oxygen gas flow and melted using two CO_2 lasers at approximately 2000 °C. The melt was rapidly solidified by shutting off the lasers at a cooling rate of approximately 300 °C/s in order to obtain fully vitrified samples. The obtained spherical glasses (2 mm in diameter) were colorless and transparent. Glass formation was confirmed via Cu $K\alpha$ XRD analysis (Rigaku, RINT 2000). In order to rule out any compositional changes of the glass during the melting process, X-ray fluorescence experiments (JEOL, JSX-3100RII) were performed on glass samples under vacuum conditions. Glasses with composition $40Y_2O_3$-$55Al_2O_3$-$5SiO_2$, $28.5La_2O_3$-$71.5Al_2O_3$, and $29.3Al_2O_3$-$50.2SiO_2$-$20.5Sc_2O_3$ were also fabricated using the levitation technique for comparative purposes.

Scanning transmission electron microscopy observation. In order to verify the homogeneity of the fabricated glasses observation with a scanning transmission electron microscope (JEOL, ARM-200CF) coupled with a high-angle annular dark field (HAADF) detector was performed. The microscope was equiped with a spherical aberration corrector (Ceos, Gmbh) and a cold field emission gun was used. The probe-forming aperture angle was 24.5 mrad while the HAADF and bright field (BF) detectors spanned through 68–280 and 0–17 mrad respectively. The spatial resolution of the present observation was approximately 0.1 nm. Glass powders were dropped into a perforated amorphous carbon films supported in Cu grids. No sputtering or heating was applied to the samples prior to the observation.

Thermal and physical properties. The glass transition temperature T_g and crystallization temperature T_p were determined via DTA at a heating rate of 10 °C/s (SII, TG6300). Prior to the analysis of the physical and structural properties, the glasses were annealed at 10 °C above the T_g in order to relax the stress introduced during quenching. The density ρ was determined using gas pycnometry (Micrometrics, AccuPyc II 1340). The experimental error associated with the density measurements was smaller than 0.01 g/cm^3. The experimental densities for the $40Y_2O_3$-$55Al_2O_3$-$5SiO_2$, $28.5La_2O_3$-$71.5Al_2O_3$ and $29.3Al_2O_3$-$50.2SiO_2$-$20.5Sc_2O_3$ glasses were 4.95 g/cm^3, 4.22 g/cm^3 and 3.04 g/cm^3 respectively. The transmittance spectrum of an approximately 300 μm-thick sample was obtained in the range from 200 nm to 800 nm using a UV/vis spectrometer (Shimadzu, UV3100PC). The refractive index dispersion was determined via spectroscopic ellipsometry (J. A. Woolam, M-2000U).

Elastic moduli measurement. The pulse-echo overlap technique was used to obtain the ultrasonic velocities of the glass[39]. A 50 μm-thick ultrasonic transducer ($LiNbO_3$ 10 °Y-cut) and a 300 μm-thick glass were pasted at opposite corners of an edge truncated tungsten carbide (WC) block using a conductive epoxy resin. The ultrasonic echoes of the longitudinal P and shear S waves from the transducer were reflected by the glass and observed using a digital oscilloscope. The longitudinal velocity V_P and transversal velocity V_S were determined by dividing the thickness of the samples by the observed travel time of the waves. The longitudinal modulus L (C_{11}) and shear modulus G (C_{44}) were estimated using the equations $L = V_P^2$ and $G = V_S^2$. The Young's modulus E, bulk modulus K, and Poisson's ratio ν were calculated using the equations $E = G(3L - 4G)/(L - G)$, $K = L - (4/3)G$, and $\nu = (L - 2G)/(L - G)$, respectively. The obtained Young's modulus E for the $40Y_2O_3$-$55Al_2O_3$-$5SiO_2$, $28.5La_2O_3$-$71.5Al_2O_3$ and $29.3Al_2O_3$-$50.2SiO_2$-$20.5Sc_2O_3$ glasses were 145.6 GPa, 123 GPa and 133.2 GPa respectively.

Indentation behavior. Indentation experiments were performed on a Shimazu DUH HMV-1 Vickers tester at 23 °C and approximately 60% relative humidity. Optical-grade polished samples with a thickness of approximately 500 μm were used. The dwell time was set at 15 s. The Vickers hardness values H_V were calculated from the diagonal lengths of the imprints at a load of 0.980 N. At least 20 indents were made for measuring H_V. The indentation cracking resistance CR values were estimated from cracking probability curves using the method proposed by Wada *et al.*[40]. Here, CR is defined as the load required to generate two radial cracks on average or to achieve a 50% cracking probability. Each data point on the cracking probability curves developed in the present study also represents 20 indentation imprints. The reported value of CR was obtained by averaging the CR values determined from sigmoidal fittings of the cracking probability curves for three different samples. The imprints were observed by optical microscopy.

Al local structure. ^{27}Al MAS NMR spectroscopy of the glass was performed on a JEOL JNM-ECA 500 spectrometer equipped with MAS probe head at 11.74 T (500 MHz). The spinning rate was 15 kHz, and a 4-mm-diameter zirconia rotor was used. The NMR spectra were recorded using $\pi/6$ pulses (0.4 μs) and a relaxation delay of 1 s, and 4000–12000 signals were accumulated. The ^{27}Al chemical shift δ_{iso} in parts per million (ppm) was referenced to an external 1 M $AlCl_3$ solution (−0.1 ppm).

References

1. Rouxel, T. Elastic properties and short-to medium-range order in glasses. *J. Am. Ceram. Soc.* **90,** 3019–3039 (2007).

2. Wallenberger, F., Brown, S. D. & Onoda, G. Y., Jr. ZnO-modified high modulus glass fibers. *J. Non-Cryst. Solids* **152,** 279–283 (1993).
3. Seghal, J. & Ito, S. A new low-brittleness glass in the soda-lime-silica glass family. *J. Am. Ceram. Soc.* **81,** 2485–2488 (1998).
4. Makishima, A. & Mackenzie, J. D. Direct calculation of Young's modulus of glass. *J. Non-Cryst. Solids* **12,** 35–45 (1973).
5. Makishima, A. & Mackenzie, J. D. Calculation of bulk modulus, shear modulus and Poisson's ratio of glass. *J. Non-Cryst. Solids* **17,** 147–157 (1975).
6. Inoue, H., Masuno, A., Watanabe, Y., Suzuki, K. & Iseda, T. Direct calculation of the physical properties of sodium borosilicate glass from its chemical composition using the concept of structural units. *J. Am. Ceram. Soc.* **95,** 211–216 (2012).
7. Yamane, M. & Mackenzie, J. D. Vicker's hardness of glass. *J. Non-Cryst. Solids* **15,** 153–164 (1974).
8. Stevensson, B. & Edén, M. J. Structural rationalization of the microhardness trends of rare-earth aluminosilicate glasses: interplay between the RE^{3+} field-strength and the aluminum coordinations. *J. Non-Cryst. Solids* **378,** 163–167 (2013).
9. Johnson, J., Weber, R. & Grimsditch, M. Thermal and mechanical properties of rare-earth aluminate and low-silica aluminosilicate optical glasses. *J. Non-Cryst. Solids* **351,** 650–655 (2005).
10. Du, J. Molecular dynamics simulations of the structure and properties of low silica yttrium aluminosilicate glasses. *J. Am. Ceram. Soc.* **92,** 87–95 (2009).
11. Inaba, S., Todaka, S., Ohta, Y. & Morinaga, K. Equation for estimating the Young's modulus, shear modulus and Vickers hardness of aluminosilicate glasses. *Nippon Kinzoku Gakkaishi* **64,** 177–183 (2000).
12. Sun, K. H. Fundamental condition of glass formation. *J. Am. Ceram. Soc.* **30,** 277–281 (1947).
13. Yu, J. *et al.* Fabrication of $BaTi_2O_5$ glass-ceramics with unusual dielectric properties during crystallization. *Chem. Mater.* **18,** 2169–2173 (2006).
14. Masuno, A. *et al.* Glass-forming region and high refractive index of TiO_2-based glasses prepared by containerless processing. *Phys. Status Solidi C* **9,** 2424–2427 (2012).
15. Masuno, A. & Inoue, H. High refractive index of $0.3La_2O_3-0.7Nb_2O_5$ glass prepared by containerless processing. *App. Phys. Express* **3,** 102601–3 (2010).
16. Masuno, A., Kohara, S., Hannon, A. C., Bychkov, E. & Inoue, H. Drastic connectivity change in high refractive index lanthanum niobate glasses. *Chem. Mater.* **25,** 3056–3061 (2013).
17. Yoshimoto, K., Masuno, A., Inoue, H. & Watanabe, Y. Transparent and high refractive index $La_2O_3-WO_3$ glass prepared by containerless processings. *J. Am. Ceram. Soc.* **95,** 3501–3504 (2012).
18. Watanabe, Y., Masuno, A. & Inoue, H. Glass formation of rare-earth aluminates by containerless processing. *J. Non-Cryst. Solids* **358,** 3563–3566 (2012).
19. Weber, R., Nordine, P., Key, T. & Tangeman, J. Device materials based on Er-, Ho-, Tm-, Yb-doped rare earth aluminum oxide (REAl) glass. *Proc. SPIE* **4990,** 70–76 (2003).
20. Rosenflanz, A. *et al.* Bulk glasses and ultrahard nanoceramics based on alumina and rare-earth oxides. *Nature* **430,** 761–764 (2004).
21. Mizoguchi, T. *et al.* Atomic-scale identification of individual lanthanide dopants in optical glass fiber. *ACS Nano* **7,** 5058–5063 (2013).
22. Apetz, R. & van Bruggen, M. P. B. Transparent alumina: a light-scattering model. *J. Am. Ceram. Soc.* **86,** 480–486 (2003).
23. Masuno, A., Inoue, H., Yu, J. & Arai, Y. Refractive index dispersion, optical transmittance, and Raman scattering of $BaTi_2O_5$ glass. *J. Appl. Phys.* **108,** 063520–5 (2010).
24. Pahari, B. *et al.* Composition-property-structure correlations of scandium aluminosilicate glasses revealed by multinuclear ^{45}Sc, ^{27}Al, and ^{29}Si solid-state NMR. *J. Am. Ceram. Soc.* **95,** 2545–2553 (2012).
25. Sehgal, S. J. & Ito. Brittleness of glass. *J. Non-Cryst. Solids* **253,** 126–132 (1999).
26. Kurjian, C. R., Kammlott, K. G. & Chaudhri, M. M. Indentation behavior of soda-lime glass, fused silica, and single-crystal quartz at liquid nitrogen temperature. *J. Am. Ceram. Soc.* **78,** 737–744 (1995).
27. Gross, T. M., Tomozawa, M. & Koike, A. A glass with high crack initiation load: role of fictive temperature-independent mechanical properties. *J. Non-Cryst. Solids.* **355,** 563–568 (2009).
28. Schmücker, M., Schneider, H., Mackenzie, K. J. D. & Okuno, M. Comparative ^{27}Al NMR and LAXS studies on rapidly quenched aluminosilicate glasses. *J. Eur. Ceram. Soc.* **19,** 99–103 (1999).
29. Neuville, D. R., Cormier, L. & Massiot, D. Al coordination and speciation in calcium aluminosilicate glasses: effects of composition determined by ^{27}Al MQ-MAS NMR and Raman spectroscopy. *Chem. Geol.* **229,** 173–185 (2006).
30. Licheron, M., Montouillout, V., Millot, F. & Neuville, D. R. Raman and ^{27}Al NMR structure investigations of aluminate glasses: $(1-x)Al_2O_3$-xMO, with M = Ca, Sr, Ba and $0.5 < x < 0.75$. *J. Non-Cryst. Solids.* **357,** 2796–2801 (2011).
31. Massiot, D. *dm fit program* (2002). URL http://crmht-europe.cnrs-orleans.fr. (Accessed: 15th February 2015).
32. d'Epinose de Lacaillerie, J. B., Fretigny, C. & Massiot, D. MAS NMR spectra of quadrupolar nuclei in disordered solids: The Czjzek model. *J. Magn. Reson.* **192,** 244–251 (2008).
33. Neuville, D. R., Cormier, L. & Massiot, D. Al environment in tectosilicate and peraluminous glasses:A ^{27}All MQ-MAS NMR, Raman and XANES investigation. *Geochim. Cosmochim. Acta* **68,** 5071–5079 (2004).
34. Takahashi, S., Neuville, D. R. & Takebe, H. Thermal properties, density and structure of percalcic and peraluminus CaO-Al_2O_3-SiO_2 glasses. *J. Non-Cryst. Solids* **411,** 5–12 (2015).
35. Tangeman, J. A., Phillips, B. L., Nordine, P. C. & Weber, J. K. R. Thermodynamics and structure of single- and two-phase yttria-alumina glasses. *J. Phys. Chem. B* **108,** 10663–10671 (2004).
36. Shannon, R. D. & Prewitt, C. T. Effective ionic radii in oxides and fluorides. *Acta Crystallogr.* **25,** 925–946 (1969).
37. Inaba, S., Fujino, S. & Morinaga, K. Young's modulus and compositional parameters of oxide glasses. *J. Am. Ceram. Soc.* **82,** 3501–3507 (1999).
38. Swarnakar, A. K., Stamboulis, A., Holland, D. & Van der Biest, O. Improved prediction of Young's modulus of fluorine-containing glasses using MAS-NMR structural data. *J. Am. Ceram. Soc.* **96,** 1271–1277 (2013).
39. Higo, Y., Kono, Y., Inoue, T., Irufune, T. & Funakoshi, K. A system for measuring elastic wave velocity under high pressure using a combination of ultrasonic measurement and the multi-anvil apparatus at Spring-8. *J. Synchrotron Radiat.* **16,** 762–768 (2009).
40. Wada, M., Furukawa, H. & Fujita, K. Crack resistance of glass on vickers hardness. *Proc. Int. Congr. Glass, 10th.* **11,** 39–46 (1974).

Acknowledgements

This work was supported in part by The Kazuchika Okura Memorial Foundation, Grant for Basic Science Research Projects from The Sumitomo Foundation, and Grant-in-Aid for Scientific Research (25410236 and 26630302) from the Ministry of Education, Culture, Sports and Science and Technology of Japan.

Author Contributions

G.A.R.S. wrote the manuscript, analyzed the results, fabricated the glasses and conducted the indentation experiments, A.M. wrote the manuscript, organized the research and analyzed the results, Y.H. conducted the elastic moduli measurement, Y.Y. conducted the ^{27}Al MAS NMR experiments, T.M. conducted the scanning transmission electron microscopy observations, H.I., T.U., K.O., K.K. and Y.W. discussed the results. All authors reviewed the manuscript.

Additional Information

Competing financial interests: The authors declare no competing financial interests.

How to cite this article: Rosales-Sosa, G. A. *et al.* High Elastic Moduli of a $54Al_2O_3$-$46Ta_2O_5$ Glass Fabricated via Containerless Processing. *Sci. Rep.* **5**, 15233; doi: 10.1038/srep15233 (2015).